# Physics based lumped element circuit model for nanosecond pulsed dielectric barrier discharges

Thomas Underwood,[1,a)] Subrata Roy,[1,b)] and Bryan Glaz[2]

[1]*Applied Physics Research Group, Department of Mechanical and Aerospace Engineering, University of Florida, Gainesville, Florida 32611, USA*
[2]*Vehicle Technology Directorate, U.S. Army Research Laboratory, Aberdeen Proving Ground, Maryland 21005, USA*

This work presents a physics based circuit model for calculating the total energy dissipated into neutral species for nanosecond pulsed direct current (DC) dielectric barrier discharge (DBD) plasmas. Based on experimental observations, it is assumed that the nanosecond pulsed DBD's which have been proposed for aerodynamic flow control can be approximated by two independent regions of homogeneous electric field. An equivalent circuit model is developed for both homogeneous regions based on a combination of a resistor, capacitors, and a zener diode. Instead of fitting the resistance to an experimental data set, a formula is established for approximating the resistance by modeling plasmas as a conductor with DC voltage applied to it. Various assumptions are then applied to the governing Boltzmann equation to approximate electrical conductivity values for weakly ionized plasmas. The developed model is then validated with experimental data of the total power dissipated by plasmas. © *2013 American Institute of Physics*. [http://dx.doi.org/10.1063/1.4792665]

## I. INTRODUCTION

The need for improved control over aerodynamic flow separation has increased interest in the potential use of plasma actuators. The inherent advantages of plasma actuator flow control devices include: fast response time, surface compliance, lack of moving parts, and inexpensiveness. However, it has been established that the actuators which affect the flow via directed momentum transfer are not effective at Mach numbers associated with most subsonic aircraft applications. Recently, Roupassov *et al.*[1] demonstrated that pulsed plasma actuators, in which energy imparted to the flow appears to effectively control flow separation, seem to be suitable at Mach numbers (M ≈ 0.3) beyond the capabilities of the current plasma induced momentum based approaches.

Given the fundamental differences between the novel pulsed discharge approach and the more conventional momentum based approaches, there is a need to develop an effective and efficient model for the energy delivered to the flow by the plasma. Once calculated, that value can be input to a computational fluid dynamics solver as an energy source term resulting in a coupled fluid/plasma dynamics model. Multiphysics models of this type are required in order to study detailed flow characteristics. However, detailed numerical simulations involving plasma kinetics are computationally prohibitive for a variety of coupled fluid/plasma design problems. To address this issue, efficient circuit element models have been introduced to approximate the complex processes within plasmas. Circuit models such as those by Orlov[2] rely on empirical constants which may not be applicable to nanosecond pulsed discharges. To date, an approximate model of nanosecond pulsed plasma actuators has not been developed. This paper deals primarily with establishing a flexible model with relevant physics that could be implemented as an approximation for the energy dissipated within a plasma for any pulsed direct current (DC) dielectric barrier discharge (DBD) configuration. Among the other goals in this paper is to probe into the background processes that occur within plasmas and incorporate that knowledge into the model.

## II. LUMPED ELEMENT CIRCUIT MODEL

One of the primary assumptions in creating this model is that nanosecond pulsed DBD's can be approximated by two independent regions of homogeneous electric field. One such region, dubbed the "hot spot" is the region adjacent to the powered electrode. This region makes up a small portion of the total discharge area but was observed to be an important component of the plasma discharge and necessary to obtain agreement with experimentally measured shock wave dynamics by Roupassov *et al.*[1] The other region, dubbed the "tail," encompasses the rest of the plasma discharge and extends to the edge of the dielectric. As both regions are independent, the model presented in this paper consists of a single network for each region containing a resistor, capacitors, and a diode.

As shown in Fig. 1, circuit elements that were used to model the plasma include: an air capacitor $C_a$, a dielectric capacitor $C_d$, a resistor $R_f$, and a zener diode $D_f$. The air capacitor represents the capacitance between the dielectric surface and the exposed electrode. The dielectric capacitor represents the capacitance between the dielectric surface and insulated electrode and is proportional to the thickness of the dielectric layer. Thus, the dielectric layer in the form of both its thickness and the value of its dielectric constant plays an important role in determining the effectiveness of the plasma actuator. Finally, the zener diode, introduced by Orlov[2] is utilized in the model to enforce an energy threshold value below which plasma will not form.

a)Undergraduate Student.
b)Electronic mail: roy@ufl.edu. URL: http://aprg.mae.ufl.edu/roy/.
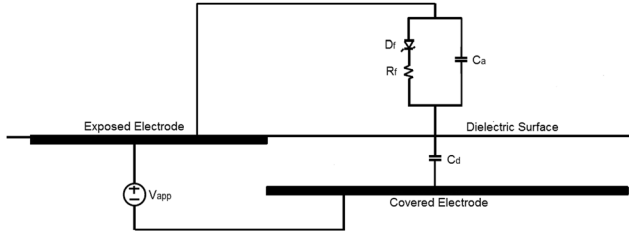
FIG. 1. Electric circuit model of a dielectric aerodynamic plasma actuator.

Since a uniform charge distribution along the top of the dielectric is assumed, the typical asymmetric 2D plasma actuator geometry featured in Fig. 1 can be simplified to a series of homogeneous symmetric regions. As shown in Fig. 2, these regions include: an anode sheath, "hot spot," and "tail." This assumption results in a series of coupled 1D models that account for the chordwise variation along the actuator. Fig. 3 shows the simplified circuit model within each homogeneous region.

## A. Circuit

As displayed in Fig. 1, the lumped element circuit is a function of the two capacitance values, $C_a$ and $C_d$. In this model, the air is treated as both a conductor to generate a physical relationship for the resistance $R_f$ and a parallel plate capacitor to generate $C_a$. An advantage of modeling the plasma as a conductor in addition to a parallel plate capacitor is that it generates a physical relationship for the resistance, $R_f$, a value that is traditionally empirically determined. The air gap capacitor can be modeled as[3]

$$C_a = \frac{\epsilon_0 \epsilon_a A_a}{h_a}, \tag{1}$$

where $A_a$ is the cross-sectional area of the air and $h_a$ is the approximate height of the plasma region of interest. The height of the plasma has been shown by Roupassov et al.[1] to be approximately independent of applied voltage for nanosecond pulsed DBD actuators. As displayed in Fig. 4, $A_a$ is the product of the spanwise length of the actuator $z_a$ and $l_a$, the chordwise distance from the exposed electrode to the end of the dielectric region.

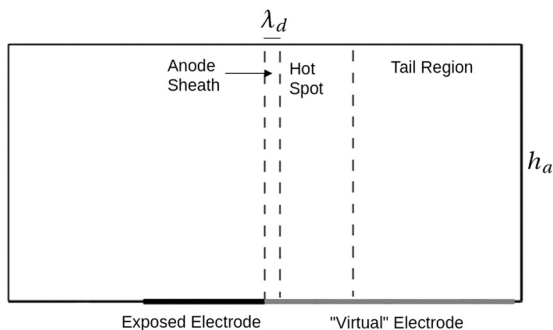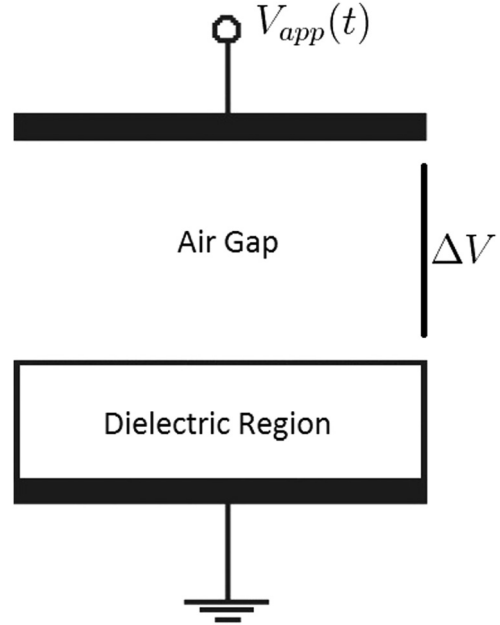The capacitive element corresponding to the dielectric can be modeled as[3]



FIG. 3. Region of homogeneous potential, i.e., "hot spot."

$$C_d = \frac{\epsilon_0 \epsilon_d A_d}{h_d}, \tag{2}$$

where $A_d$ is the cross-sectional area of the dielectric capacitive element and $h_d$ is the height of the dielectric barrier layer. As displayed in Fig. 5, $A_d$ is the product of the spanwise length of the actuator $z_a$ and $d_d$, the width of the dielectric region.

Treating the plasma as a conductor, the resistance for DC voltage is proportional to $\sigma_p$, $A_a$, and $h_a$. It can be given as[3]

$$R_f = \frac{h_a}{\sigma_p A_a}. \tag{3}$$

Starting from Kirchoff's circuit laws,[3] the governing differential equation for the voltage drop experienced by the air gap, $\Delta V$, is given by

$$\frac{d\Delta V(t)}{dt} = -\frac{dV_{app}}{dt}\left(\frac{C_a}{C_a + C_d} - 1\right) - \kappa \frac{\Delta V(t)}{R_f(t)(C_a + C_d)}, \tag{4}$$

$$\kappa = \begin{cases} 1 & \text{if } |\boldsymbol{E}| > E_{crit} \\ 0 & \text{if } |\boldsymbol{E}| \leq E_{crit}, \end{cases} \tag{5}$$

where $V_{app}$ is the applied voltage and $\kappa$ is the contribution from the zener diode. If the electric field magnitude, given as
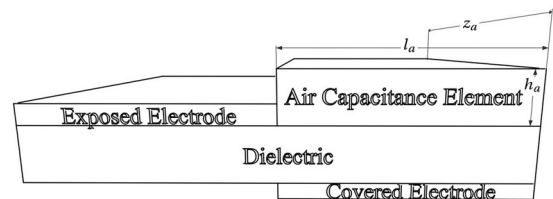


FIG. 2. Plasma discharge regions analyzed in this study.



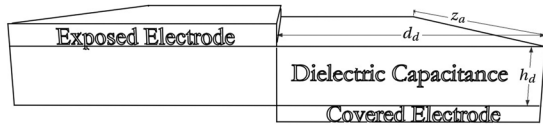FIG. 4. Sketch of the capacitive air element.

FIG. 5. Sketch of the dielectric capacitive element.

$$|\boldsymbol{E}| = \frac{|\Delta V|}{h_a}, \tag{6}$$

is greater than the breakdown electric field,[2] $E_{crit}$, required to ionize air, then $\kappa$ takes on a value of one, otherwise it is zero to signify that plasma has not formed.

## B. Conductivity

To effectively calculate the resistance governed by Eq. (3), an expression must first be developed for the electrical conductivity, $\sigma_p$, of the plasma. This value is one that traditionally requires a numerical approach. To simplify the problem to a point where an analytic formulation can be used, numerous simplifying assumptions were used and are described in the following paragraphs.

For any plasma, the resulting electric current is composed of two primary terms: the current from electrons and that from ions. As the drift velocity of electrons, $\boldsymbol{w_e}$, in a non-equilibrium plasma is significantly higher than ions, the current density can be approximated as the portion from electrons if the number densities, $N_e$ and $N_i$, are approximately the same. Using a form of the generalized Ohm's Law, the current density vector, $\boldsymbol{J}$ and $\sigma_p$, respectively, can be written as

$$\boldsymbol{J} \approx -eN_e\boldsymbol{w_e} = \sigma_p\boldsymbol{E}, \tag{7}$$

$$\sigma_p = e(N_e\mu_e + N_i\mu_i), \tag{8}$$

where $\mu_i$ and $\mu_e$ represent the ion and electron mobilities, respectively. Much like Eq. (7), the electrical conductivity relation can be simplified using the concept of quasineutrality which is defined as having approximate equal number densities for charged particles of opposite polarity. Thus, as $\mu_e$ is typically three orders of magnitude larger than $\mu_i$, it is a good assumption to approximate the electrical conductivity as only coming from electrons as long as $N_e$ is at least of the same order of magnitude as $N_i$.[4] Quasineutrality is a typical assumption that is valid as long as the plasma being modeling is far enough away from the powered electrode to avoid the boundary layer in plasma physics called the sheath.

Since a pulsed DC voltage is assumed, the activation of the external electric field will follow the voltage waveform as a step function. Thus, two expressions will be required for $\sigma_p$, where the first is valid for the period when an external electric field is applied, as shown in Fig. 9 from 0 to 60 ns, and the second when the voltage drop over the air gap is zero. For the portions of the voltage waveform that $\Delta V$ is zero, the power is also zero according to Ohm's Law and thus the conductivity during this time is of no importance.

To generate a analytic formula for the electrical conductivity, a distribution function must be introduced to describe

the physical evolution in the number of particles, $f(\boldsymbol{v}, J, \boldsymbol{r}, t)$, defined such that $f(\boldsymbol{v}, J, \boldsymbol{r}, t)\,d\boldsymbol{v}$ is the number of particles in a unit volume located at point $\boldsymbol{r}$, time $t$, internal quantum number $J$, and differential velocity range $\boldsymbol{v} + d\boldsymbol{v}$. Using this distribution function, the number of particles at point $\boldsymbol{r}$ and time $t$ can be defined as

$$N(\boldsymbol{r}, t) = \sum_J \int f(\boldsymbol{v}, J, \boldsymbol{r}, t)d\boldsymbol{v}. \tag{9}$$

This distribution function allows a mathematical description to be developed for the temporal evolution in the number of particles resulting from particle collisions within a control volume. The time rate of change in the number of particles due to externally applied fields can be described as[5]

$$\frac{Df}{Dt} = \frac{f(\boldsymbol{v} + d\boldsymbol{v}, J, \boldsymbol{r} + d\boldsymbol{r}, t + dt) - f(\boldsymbol{v}, J, \boldsymbol{r}, t)}{dt}. \tag{10}$$

A partial differential equation can be developed to describe Eq. (10) using formulas for the time rate of change of $\boldsymbol{v}$ and $\boldsymbol{r}$ established using the equation of motion in the form of

$$\frac{d\boldsymbol{v}}{dt} = \frac{\boldsymbol{F}}{m}, \tag{11}$$

$$\frac{d\boldsymbol{r}}{dt} = \boldsymbol{v}, \tag{12}$$

and the chain rule of calculus to obtain the Boltzmann kinetic energy equation given as

$$\frac{Df}{Dt} = \frac{\partial f}{\partial t} + \boldsymbol{v} \cdot \frac{\partial f}{\partial \boldsymbol{r}} + \frac{\boldsymbol{F}}{m} \cdot \frac{\partial f}{\partial \boldsymbol{v}}. \tag{13}$$

In order to approximate the total derivative, a relaxation time can be introduced defined as the time taken for the system to be reduced to an equilibrium distribution function. The tau approximation can be given as $\tau \approx (N_a\sigma_{ea}|\boldsymbol{v}|)^{-1}$, where $\sigma_{ea}$ is the collision cross section between electrons and atoms, $\boldsymbol{v}$ is the average collision velocity, and $N_a$ is the number density of atoms.[5] If the number of particles within a control volume is defined as a equilibrium distribution function, $f_0$, when each particle is at the same energy level as its neighbor, then the particle evolution over time due to pairwise collisions after an external force has been applied can be given as[5]

$$\frac{Df}{Dt} = -\frac{f - f_0}{\tau}. \tag{14}$$

As $\tau$ only accounts for collisions between electrons and neutral atoms, it is only accurate in the event of weakly ionized plasma. Plasma actuators considered in this paper traditionally feature a low degree of ionization, or simply the amount of air that is ionized, and thus can be treated in a weakly ionized limit. In terms of the momentum-transfer collision frequency which can be defined as the mass corrected rate at which a particle of a specific species collides with another, the criteria for a weakly ionized plasma can be given as[4]

$$\bar{\nu}_{ei} \ll \bar{\nu}_{en}. \tag{15}$$

This equation requires that the collision frequency between electrons and ions be much less than those between electrons and neutrals. Thus, if this requirement is met, the collisional occurrences between electrons and charged particles can be effectively ignored and the relaxation time established is a good approximation of the total time rate of change in the number of particles within a control volume.

After introducing a relaxation time to approximate Eq. (13), an equation of motion describing the average velocity of electrons can be established by multiplying by $m_e \boldsymbol{v}$ and integrating over the electron velocity. An analytic formulation for the average velocity an electron experiences due to an externally applied field, $\boldsymbol{w}_e$, can be obtained by assuming that the force term can be approximated as the Lorentz force

$$\boldsymbol{F} = -e\boldsymbol{E} - \frac{e}{c}(\boldsymbol{v} \times \boldsymbol{B}), \tag{16}$$

where $\boldsymbol{B}$ represents the magnetic field and $\boldsymbol{E}$ represents the electric field. As plasma actuators have no applied magnetic field, $\boldsymbol{B}$ can be set equal to zero. Therefore, the equation of motion for an electron describing $\boldsymbol{w}_e$ can be given as

$$\frac{m_e d\boldsymbol{w}_e(t)}{dt} + \frac{m_e \boldsymbol{w}_e(t)}{\tau} = -e\boldsymbol{E}(t). \tag{17}$$

Solving Eq. (17), a linear first-order differential equation, an integral equation is obtained

$$w_e(t^*) = -\frac{e}{m_e}\exp\left(-\frac{t^*}{\tau^*}\right)\int_0^{t^*} E(t)\exp\left(-\frac{t^*}{\tau^*}\right) \, dt. \tag{18}$$

Equation (18) can be solved in conjunction with Eq. (7) to obtain an expression for the time varying conductivity and in conjunction with Eq. (8) to obtain an approximation for the time varying electron mobility if the ion mobility is neglected. The electrical conductivity and electron mobility, respectively, can be given as

$$\sigma_p(t^*) = \frac{N_e(t^*)e^2}{m_e E(t^*)}\int_0^{t^*} E(t)\exp\left(\frac{t - t^*}{N_a^* \sigma_{ea}^* \nu^*}\right) \, dt, \tag{19}$$

$$\mu_e(t^*) \approx \frac{e}{m_e E(t^*)}\int_0^{t^*} E(t)\exp\left(\frac{t - t^*}{N_a^* \sigma_{ea}^* \nu^*}\right) \, dt, \tag{20}$$

where $\sigma_{ea}$ is a function of electron energy and can be obtained for various molecules found in air from Phelps.[6] Numerical values used in the model are included in the Appendix. The electron velocity can be obtained by assuming a Maxwellian velocity profile. As a collection of electrons within plasma have a range of velocities, the Maxwellian velocity profile represents the most probable distribution of these velocities. Thus, the distribution of velocities, $f(u, v, w)$, can be given by[4]

$$f(u, v, w) = A_3 \exp\left[-\frac{\frac{1}{2}m(u^2 + v^2 + w^2)}{k_b T_e}\right], \tag{21}$$

$$A_3 = N_e\left(\frac{m}{2\pi k_b T_e}\right)^{\frac{1}{2}}. \tag{22}$$

Using the non-relativistic definition of kinetic energy, a relationship can be established for the kinetic energy of an electron that is valid in the limit $|\boldsymbol{v}| \ll c$, where $c$ is the speed of light. Using this approximation, the relativistic formulation of the kinetic energy can be approximated as

$$E_k = \frac{mc^2}{\sqrt{1 - |\boldsymbol{v}|^2/c^2}} - mc^2 \approx \frac{1}{2}m\boldsymbol{v}^2. \tag{23}$$

Averaging Eq. (21) and using the non-relativistic definition of kinetic energy, the mean kinetic energy of electrons becomes[4]

$$E_{av} = \frac{\iiint_{-\infty}^{\infty} A_3 \frac{1}{2}m_e(u^2 + v^2 + w^2)\exp\left[-\frac{\frac{1}{2}m_e(u^2 + v^2 + w^2)}{k_b T_e}\right] \, du \, dv \, dw}{\iiint_{-\infty}^{\infty} A_3 \exp\left[-\frac{\frac{1}{2}m_e(u^2 + v^2 + w^2)}{k_b T_e}\right] \, du \, dv \, dw}, \tag{24}$$

where $k_b$ is Boltzmann's constant. From the definition of kinetic energy, the relationship between $E_{av}$ and $|\boldsymbol{v}|$ with vector components $(u, v, w)$ can be established and the average thermal velocity of electrons becomes

$$|\boldsymbol{v}| = \sqrt{\frac{3k_b T_e}{m_e}}. \tag{25}$$

The required inputs for Eqs. (19) and (20) include: $N_e$, the number density of electrons, $N_a$, the number density of atoms, and $T_e$, the temperature of the electrons. Among these values, $N_a$ can be assumed to be constant in time as the number density of atoms is significantly higher than that of free electrons.

Many other models incorporate a constant electron temperature into their model.[2,7] Using experimentally measured values of reduced electric field,[8] $E/N_a$ vs.

electron temperature as detailed in Fig. 6, this model calculates a new electron temperature at each time step by comparing the $E/N$ value experienced by the plasma, produced from using Eqs. (4)–(6), with Fig. 6. It is assumed in this paper that the effects of an applied electric field have an instantaneous, on a time scale much faster than $10^{-9}$ s, effect on electrons.

A time-varying differential equation that governs $N_e$ can be obtained from the drift-diffusion equations. The electron continuity equation that governs $N_e$ can be given by

$$\frac{\partial N_e}{\partial t} + \nabla \cdot \mathbf{\Gamma_e} = \alpha|\mathbf{\Gamma_e}| - \beta n_i n_e, \tag{26}$$

where $\mathbf{\Gamma_e}$ is called the charged species flux, $\alpha$ is the Townsend coefficient of ionization, and $\beta$ is the recombination coefficient between electron and neutral atoms. By simplifying the plasma discharge into a combination of two homogeneous regions plus an anode sheath and by invoking the irrotational property of electric fields, Eq. (26) can be simplified by ignoring any spatial variation in the number density of electrons, i.e., $\mathbf{\Gamma_e}$ becomes

$$\mathbf{\Gamma_e} \approx N_e \mu_e |\mathbf{E}|. \tag{27}$$

Assuming the number densities of electrons and ions are equal, i.e., in the quasineutral region, the electron continuity equation for air, with a composition of 80% $N_2$ and 20% $O_2$, can be written as

$$\frac{dN_e}{dt} \approx \alpha_{air}|N_e \mu_e \mathbf{E}| - 0.80\beta_{N2}N_e^2 - 0.2\beta_{02}N_e^2, \tag{28}$$

where $\alpha_{air}$ and $\beta$, respectively, can be approximated as having the form[9]

$$\alpha_{air} = Ap \exp\left(-\frac{Bp}{E}\right), \tag{29}$$

$$\beta_{N2} = 2.8 \times 10^{-7}\left(\frac{300}{T_e}\right), \tag{30}$$

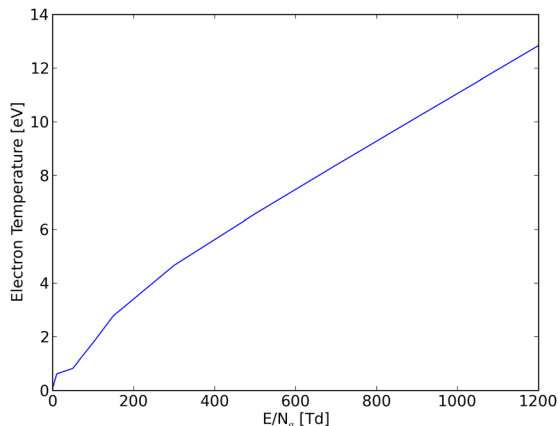$$\beta_{02} = 2 \times 10^{-7}\left(\frac{300}{T_e}\right), \tag{31}$$



FIG. 6. Plot of electron temperature vs. reduced electric field.

where A and B are empirical constants that have tabulated values of 15 and 365, respectively, for air at atmospheric pressure.[9]

## C. Discharge development

The final remaining unknown required to close the equation system is to determine how the electric potential changes over the horizontal length of the actuator. To accurately model this, it is important to incorporate the wall effects of the plasma actuator. In terms of potential variation, these wall effects attract charged particles of opposite polarity and shield charged particles of the same polarity. Therefore, for regions beside the anode (powered electrode for positive pulses), an anode sheath is developed where an attraction of electrons occurs and a repulsion of positive ions occur. For regions above the dielectric region on top of the grounded electrode, a cathode sheath is developed where positive ions are collected and electrons are repelled. Fig. 7 illustrates the two predominate sheaths that are developed in asymmetric plasma actuators.

It is important to consider the effects of charge collection and repulsion in these regions as such phenomenon can have large effects on the variation of the electric potential over the chordwise length and height of the plasma discharge.

### 1. Wall effects

As the model introduced in this paper is interested in solving for the amount of energy the plasma transfers to neutral species, the relative importance of both the anode and cathode sheath regions needs to be established. Energy, $Q$, is a function of electrical conductivity and electric field strength and can be given as

$$Q = \sigma_p|\mathbf{E}^2|V_{vol}. \tag{32}$$

Equation (32) shows that the energy transfer from both sheath regions is proportional to the conductivity of the plasma within each region. As the cathode sheath region typically has very few electrons due to repulsion effects, the current within this region will be carried by positively charged ions. The mobility of such ions are significantly less than that of an electron, so as a first order approximation if the local charged species number density and electric field strength are assumed equal, the conductivity in the cathode sheath will be significantly less than the conductivity in a bulk plasma and the anode sheath, i.e.,
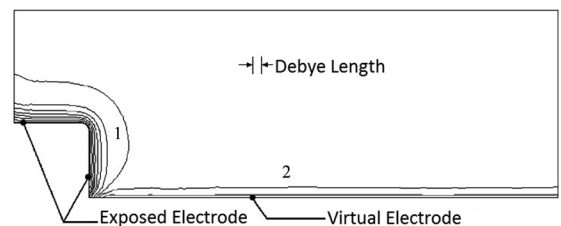


FIG. 7. Collective wall effects of the exposed powered electrode and virtual electrode (dielectric region). (1) Anode sheath and (2) cathode sheath.[12]

$$\sigma_{s-c} \ll \sigma_p \approx \sigma_{s-a}. \tag{33}$$

When combined with the fact that the volume of both sheath regions are orders of magnitude less than the bulk plasma, an order of magnitude approximation to the plasma discharge can be obtained by ignoring the cathode sheath's effects for nanosecond pulsed plasma discharges. Although the cathode sheath is approximately negligible in terms of energy transfer, the higher electric field strength and higher conductivity present in the anode sheath contain important physics necessary for capturing the energy transferred by a plasma discharge. Fig. 2 shows the updated "hot spot" and "tail" regions with the anode sheath included in the hot spot region adjacent to the powered electrode.

### 2. Electric potential variation

To establish a variation in the electric potential, the governing Maxwell equations can be used which are written as[3]

$$\nabla \cdot \mathbf{E} = \frac{\rho_f}{\epsilon_0}, \tag{34}$$

$$\nabla \cdot \boldsymbol{B} = 0, \tag{35}$$

$$\nabla \times \boldsymbol{E} = -\frac{\partial B}{\partial t}, \tag{36}$$

$$\nabla \times \boldsymbol{B} = \mu_0 \boldsymbol{J} + \mu_0 \epsilon_0 \frac{\partial E}{\partial t}, \tag{37}$$

in differential form where $\rho_f = e(n_i - n_e)$ is the net charge density and $\mu_0$ is the permeability of free space. In the absence of a time-varying magnetic field, Eq. (36), Faraday's Law of Induction, simplifies to

$$\nabla \times \boldsymbol{E} = 0, \tag{38}$$

and since the curl of $\boldsymbol{E}$ is zero, the electric field can be solved for as a potential function $\phi$ and substituted into Gauss' Law, Eq. (34). The resulting equations, respectively, can be given by

$$\mathbf{E} = -\nabla \phi, \tag{39}$$

$$\nabla^2 \phi = -\frac{\rho_f}{\epsilon}. \tag{40}$$

The net charge density within the quasineutral region of a plasma is equal to zero as $n_e = n_i$. For the anode sheath, the net charge density can be approximated if the plasma is assumed to uniformly distribute its charge density. Therefore, the quasineutral region of the "hot spot" and "tail" features

equal number densities of both electrons and ions ($n_e = n_i$), while the cathode and anode sheaths only have electron and ion densities, respectively. If this is assumed then the anode sheath can be approximated as having a net charge density equal to the quasineutral region's calculated electron number density. By assuming the anode sheath is devoid of any positive ions and has a time-dependent number density of electrons, Poisson's equation for the sheath can be given by

$$\frac{d^2 \phi}{dx^2} = \frac{e N_e(t)}{\epsilon_0}. \tag{41}$$

If this form is assumed for a single Debye length ($\lambda_D$), then the remaining discharge (rest of "hot spot" and "tail") region is part of the quasineutral bulk plasma and can be given by Laplace's equation

$$\frac{d^2 \phi}{dx^2} = 0. \tag{42}$$

The ordinary differential equations for electric potential variation in the hot spot and tail regions, respectively, can be solved to provide an approximate 1D spatial variation

$$\phi(x) = \begin{cases} \dfrac{e N_e}{2\epsilon_0} x^2 + C_1 x + C_2 & \text{if } x \le \lambda_D \\ C_3 x + C_4 & \text{if } x > \lambda_D. \end{cases} \tag{43}$$

Equation (43) requires a total of 4 boundary conditions. Those can be summarized as

$$\phi_1(x = 0) = V_{app}, \tag{44}$$

$$\phi_2(x = L) = V_{break}, \tag{45}$$

$$\phi_1(x = \lambda_D) = \phi_2(x = \lambda_D), \tag{46}$$

$$\frac{d\phi_1}{dx}(x = \lambda_D) = \frac{d\phi_2}{dx}(x = \lambda_D), \tag{47}$$

where $\phi_1$ is the potential in the anode sheath, $\phi_2$ is the potential in the quasineutral region, $L$ is length of the actuator, and $\lambda_D$ is a Debye length. The first boundary condition is $V_{app}$ at the cathode and the second is based on the experimental observations by Roupassov et al.[1] It was observed that a plasma discharge could be approximated as stopping at the edge of the grounded electrode for asymmetric actuators independent of the applied voltage; so, the edge represents the absolute limit of ionization or the breakdown voltage of air. Using Eqs. (44)–(47) as boundary conditions, the potential becomes

$$\phi(x) = \begin{cases} \dfrac{e N_e}{2\epsilon_0} x^2 + \left[ \dfrac{e N_e}{2\epsilon_0 L} \lambda_D^2 - \dfrac{e N_e}{\epsilon_0} \lambda_D + \dfrac{V_{break} - V_{app}}{L} \right] x + V_{app} & \text{if } x \le \lambda_D \\[4mm] \left[ \dfrac{e N_e}{2\epsilon_0 L} \lambda_D^2 + \dfrac{V_{break} - V_{app}}{L} \right] (x - L) + V_{break} & \text{if } x > \lambda_D. \end{cases} \tag{48}$$

The Debye length provides an order of magnitude approximation for the extent of a plasma sheath by assuming an exponential Boltzmann distribution in the charge density within the plasma discharge. Substituting this into Poisson's equation,

$$\epsilon_0 \frac{d^2\phi}{dx^2} = eN_\infty \left[ \exp\left( \frac{e\phi}{k_b T_e} \right) - 1 \right], \tag{49}$$

where $N_\infty$ is the charged particle density far away from the electrode. Taking a first-order Taylor expansion, the Debye length can be given as[4]

$$\lambda_D \sim \left( \frac{\epsilon_0 k_b T_e}{N_\infty e^2} \right)^{\frac{1}{2}}. \tag{50}$$

Although at high voltages, a first-order approximation fails, Eq. (50) still provides an order of magnitude approximation of the extent of the anode sheath.

### D. Numerical procedure

When solving for the energy imparted to neutral species, a coupled equation system results from Eqs. (4) and (28). The coupled terms include

$$R_f \propto N_e, \tag{51}$$

$$\mathbf{\Gamma_e} \propto \Delta V, \tag{52}$$

$$\beta \propto \Delta V, \tag{53}$$

$$\phi_1 \propto N_e. \tag{54}$$

To solve the resulting equation system, the Dormand-Prince Runge-Kutta method was employed. This method provides an efficient way to incorporate an adaptive step size that is important for computational efficiency in a problem that requires small time steps for convergence. The benefit of such a procedure can be illustrated through a simplistic example. If the error of each time step is defined as

$$\epsilon_k^i = y(t) - y_k^i, \tag{55}$$

then if two step sizes are considered, $h_1$ and $h_2$, the error of each iteration and their relative error, respectively, can be given as

$$y(t) - y_{n1}^1 = \epsilon_{n1}^1 = ah_1, \tag{56}$$

$$y(t) - y_{n2}^2 = \epsilon_{n2}^2 = ah_2, \tag{57}$$

$$y_{n2}^2 - y_{n1}^1 = a(h_1 - h_2). \tag{58}$$

Therefore, for a given error tolerance, $\epsilon$, a sequence of step sizes can be generated

$$h_{i+2} = q \frac{(h_i - h_{i+1})\epsilon}{|y_{n_{i+1}}^{i+1} - y_{n_i}^i|}, \tag{59}$$

TABLE I. Experimental parameters.[1]

| | |
|---|---|
| $h_a$ | 0.4 mm |
| $h_d$ | 0.3 mm |
| $\epsilon_d$ | 2.7 |
| $\epsilon_a$ | 1 |
| $A_n$ | 30 mm$^2$ |
| $A_d$ | 30 mm$^2$ |
| V | 50 kV |
| $\Delta T$ | 60 ns |

which allows a numerical ODE solver, such as those employing the Dormand-Prince method to minimize functional error by adjusting the step size after each time step.[10] Numerical integration required for Eqs. (19) and (20) and energy derived from the circuit model, given as

$$Q = \int_0^t \frac{\Delta V^2}{R_f(t)} \, dt, \tag{60}$$

were performed via the Gauss-Kronrod quadrature method[10] at each time step.

## III. RESULTS

### A. Validation against experiment

To validate the accuracy of the model described in this paper, comparisons with data presented in Roupassov et al.[1] are provided. The experimental parameters that were mentioned and used in the circuit model are given in Table I. Reference 1 uses the electrode configuration detailed in Fig. 8.

Fig. 9 illustrates an approximation of the applied voltage square wave that was introduced in the experimental work of Roupassov et al.[1] The slope that is introduced is to simulate a function that is differentiable. This is needed for $V_{app}'(t)$ in the governing differential equation as detailed by Eqs. (4) and (5). One could also generate a continuous function using Fourier decomposition of a traditional square wave; however, this would not account for the minor rise and fall times found in experimentation.
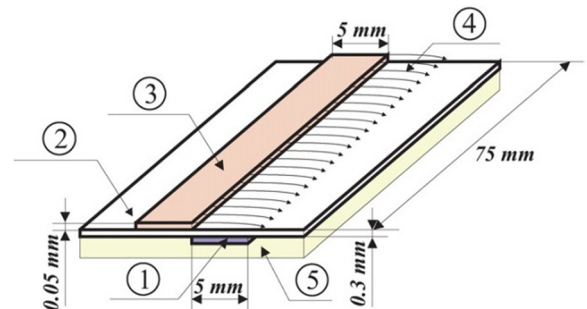


FIG. 8. Experimental scheme used by Roupassov et al.[1] for the discharge gap. (1) High-voltage electrode; (2) dielectric layer; (3) low-voltage electrode, (4) zone of discharge propagation, and (5) insulating plane.
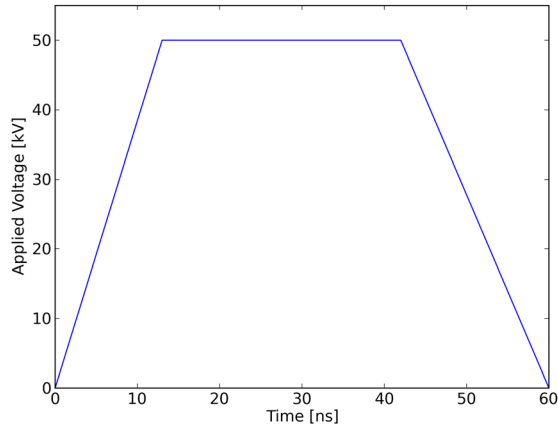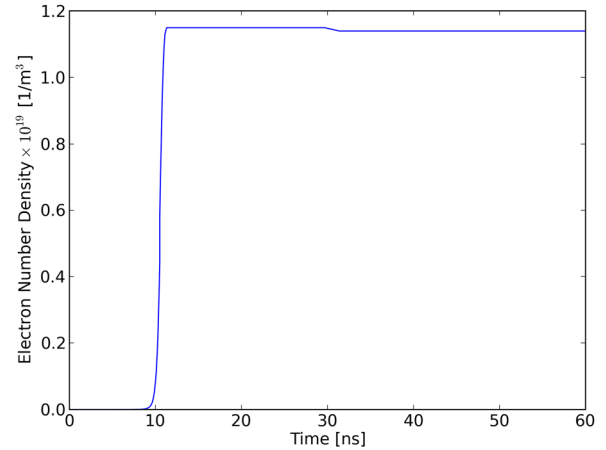
FIG. 9. Plot of the input voltage, $V_{app}$ vs. time used in the model.



FIG. 10. Plot of electron number density vs. time for the "hot spot."

## B. "Hot spot" results

For the small region of $0.4\,\text{mm} \times 0.4\,\text{mm}$ over all time outside of the anode sheath, the time variation in the number density can be established. As an initial condition for Eq. (28), $10^{15}$ m$^{-3}$ electrons were assumed based on work by Ref. 1. As displayed in Fig. 10, there is a large gradient that occurs during the rise time that peaks around $1.13 \times 10^{19}$ m$^{-3}$. It is also evident in Fig. 10 that the recombination of electrons is largely negligible on the nanosecond time scale. If a frequency of 1 kHz is used, the recombination of electrons with atoms allows a steady-state electron number density to be achieved on the nanosecond time scale. The recombination of electrons becomes a significant quantity when exploring the dynamics of a plasma discharge on the microsecond time scale.

Using Eq. (4) and Fig. 6, the model was able to produce a time-varying electron temperature. As displayed in Fig. 11, there is an initial spike in the electron temperature to 29 eV ($\approx 340\,000$ K) that coincides with the peak in electron number density at 11 ns. Fig. 11 also suggests that the assumption of a constant electron temperature is not an accurate assumption for nanosecond pulsed DBD plasmas. The variability in the electron temperature beyond 40 ns is due to the numerical error tolerances that are selected when solving Eqs. (4), (19), and (28). Fig. 11 shows that when reducing the relative error in the Dormand-Prince method from $10^{-2}$ to $10^{-3}$, the strong functional variability experiences a significant reduction. The higher the gradients are during the rise and fall time, the finer the relative error tolerances are required to be to guarantee convergence of a solution.

Using the results displayed in Figs. 10 and 11, the total power dissipated to neutral species as a function of time can be established. Using the result of Eq. (4) and the relationship for the instantaneous power, the time-varying power imparted to the flow can be given as[7]

$$P(t) = \frac{\Delta V^2(t)}{R_f(t)}. \tag{61}$$

As shown in Fig. 12, the instantaneous power is dominate during the rise time for the "hot spot" region. Upon integrating the instantaneous power over time using Eq. (60), this model produces an energy value of 2.1 mJ for this region. When compared to the experimentally determined value of 4.2 mJ by Roupassov *et al.*,[1] this model produces an order of magnitude estimate for the energy imparted to neutral species in this region.

## C. "Hot spot" sheath results

Using the Debye length approximation provided by Eq. (50) and the solution from the quasineutral "hot spot" region ($n_e \sim 10^{19}$ m$^{-3}$, $T_e \sim 10$ eV), a Debye length of 7.43 $\mu$m is generated. The electron number density experienced in the anode sheath is assumed to be equal to the values calculated in the adjacent "hot spot" region. Fig. 13 shows the time
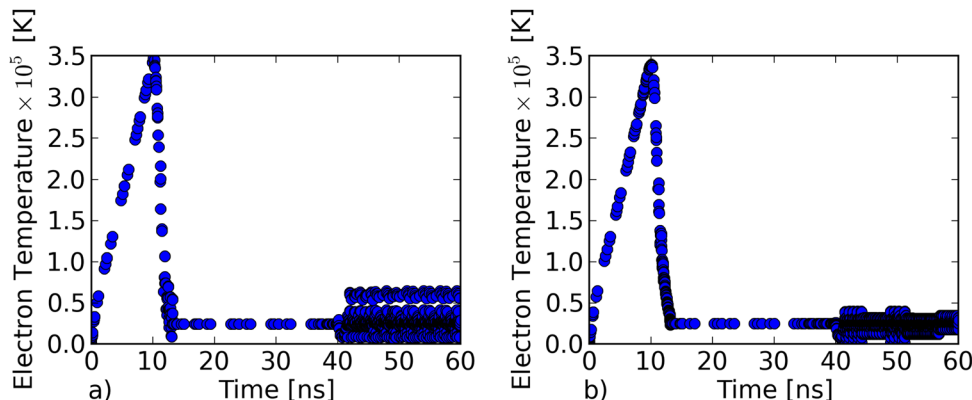


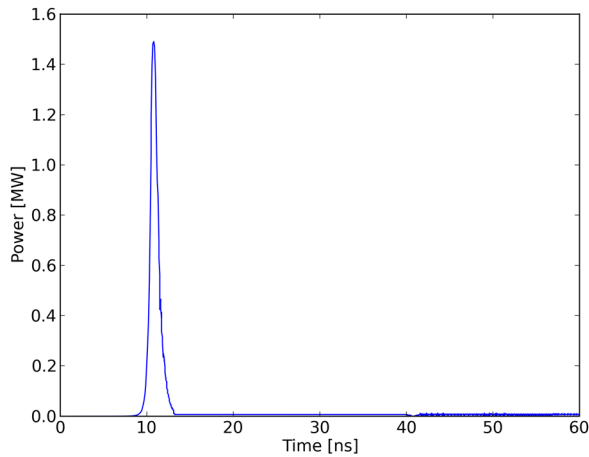FIG. 11. Plot of electron temperature vs. time for the "hot spot": (a) $10^{-2}$ error and (b) $10^{-3}$ error.

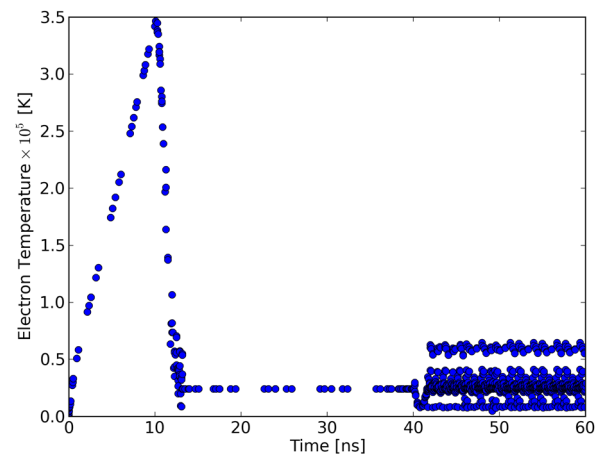FIG. 12. Plot of power vs. time for the "hot spot."



FIG. 14. Plot of electron temperature vs. time for the "hot spot" sheath.

variation in the electron number density within the sheath and also shows a peak number density of $1.13 \times 10^{19}\,\mathrm{m}^{-3}$.

Using the revised form of the electric potential within the anode sheath given by Eq. (48) and using Fig. 6, the electric temperature variation over the duration of the pulse can be established. As displayed in Fig. 14, there is an initial spike in the electron temperature to ($\approx 348\,000\,\mathrm{K}$) that coincides with the peak in electron number density at 11 ns much like the hot spot region.

As shown in Fig. 15, the instantaneous power is dominant during the rise time for the anode sheath region. Upon integrating the instantaneous power over time using Eq. (60), this model produces an energy value of 0.045 mJ for this region. This number is quite small compared to the 2.1 mJ experienced in the "hot spot" region. However, the anode sheath does have a slightly higher linear energy density than the "hot spot" region (6 J/m vs. 5.25 J/m). The reason that there is not significant deviation predicted in the anode sheath and quasineutral "hot spot" regions is that explicit charge buildup is not accounted for in the circuit model within the sheath region. As shown by Ref. 11, the electric field in the sheath and adjacent quasineutral regions are approximately equal until charge buildup is allowed within the anode sheath during the length of the pulse or a series of pulses.
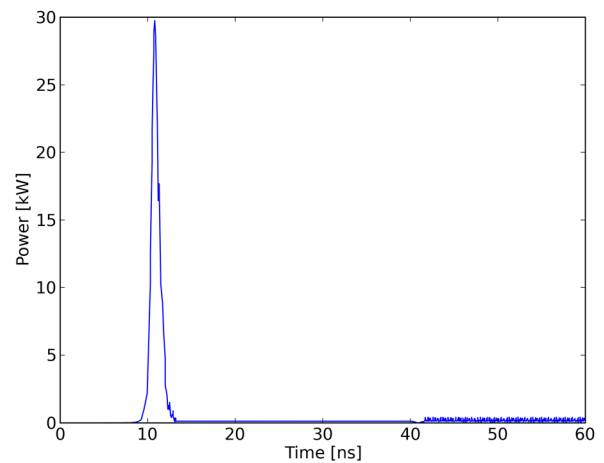


FIG. 15. Plot of power vs. time for the "hot spot" sheath.

### D. "Tail" results

For the region $0.4\,\mathrm{mm} \times 4.6\,\mathrm{mm}$, the time variation in the number density can be established. As an initial condition for Eq. (28), $10^{15}\,\mathrm{m}^{-3}$ electrons were assumed, the same number of electrons assumed for the "hot spot" region. When comparing Figs. 10 and 16, the tail region experiences a lower growth rate in the number of electrons which is due to the lower electric field experienced by this region. As described by Eq. (28), a lower electric field produces a lower
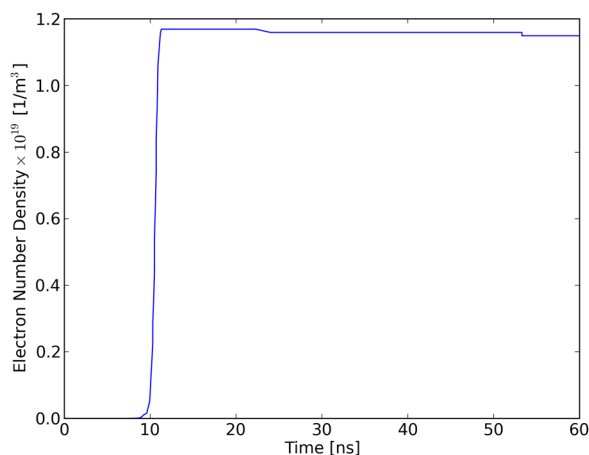


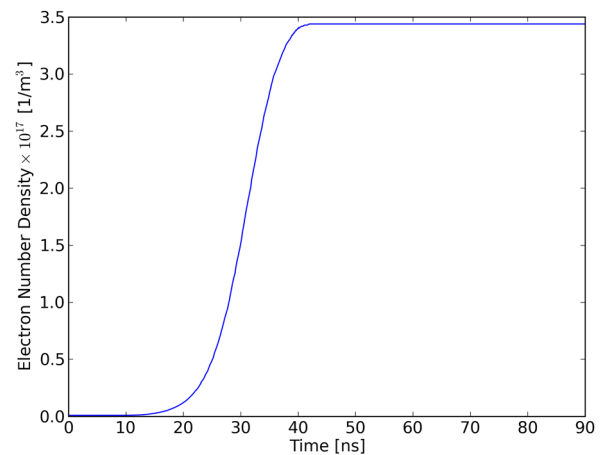FIG. 13. Plot of electron number density vs. time for the "hot spot" sheath.



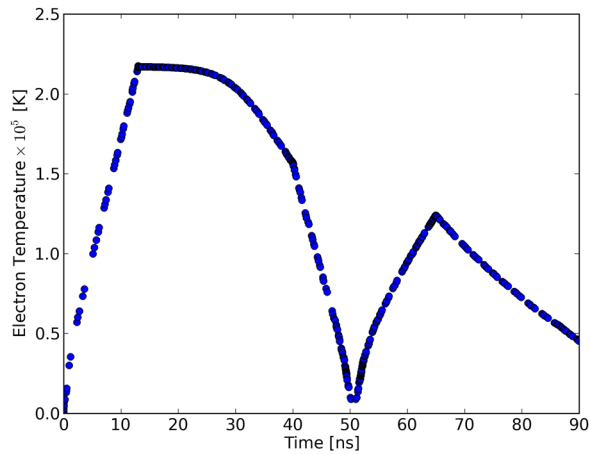FIG. 16. Plot of electron number density vs. time for the "tail."

FIG. 17. Plot of electron temperature vs. time for the "tail."

number of ionizations and therefore a more gradual rise and lower total peak in $N_e$, approximately $3.4 \times 10^{17}$ m$^{-3}$.

Using Eq. (4) and Fig. 6, the model was able to produce a time-varying electron temperature. As displayed in Fig. 17, the traditional assumption of 1 eV ($\approx$11 600 K) does not agree well with the results obtained in this model for the tail region on the nanosecond time scale. Instead, Fig. 17 suggests that the peak electron temperature is achieved during the rise time of the pulse, 220 000 K ($\approx$19 eV) and then trends downward during the plateau portion of the voltage waveform. Much like Fig. 11, the highest electron temperatures are achieved during the initial high gradient of the pulse. Fig. 17, unlike Fig. 11, also shows a rise in electron temperature during the fall time of the pulse as well. This is due to the lower electric potential and negative gradient experienced in the tail region during the fall time.

As shown in Fig. 18, the instantaneous power is dominant during the plateau portion of the applied voltage pulse for the "tail" region. Upon integrating the instantaneous power over time using Eq. (60), this model produces an energy value of 6.6 mJ. When compared to the experimentally determined value of 8 mJ by Roupassov et al.,[1] this model produces an absolute error of $\approx$17.5%. The significant improvement in
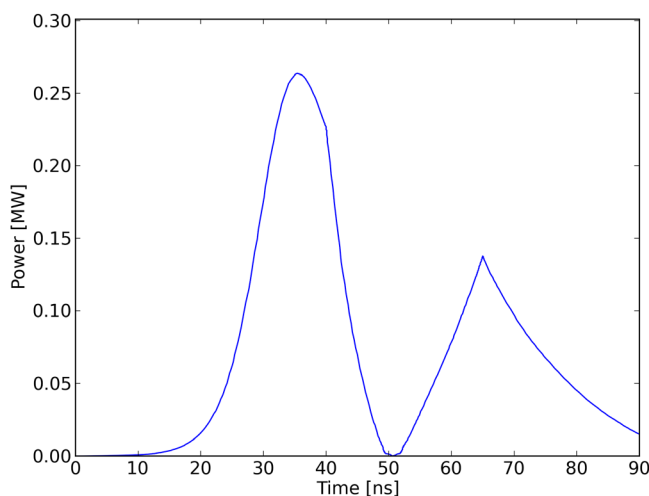


FIG. 18. Plot of power vs. time for the "tail."

TABLE II. Comparison between calculated and experimentally measured energy deposition.

|          | Circuit model (mJ) | Experimental[1] (mJ) | Abs. error (%) |
|----------|--------------------|----------------------|----------------|
| Hot spot'| 2.1                | 4.2                  | 50             |
| Tail'    | 6.6                | 8                    | 17.5           |
| Total    | 8.7                | 12.2                 | 28.7           |

accuracy for the tail region can likely be attributed to the larger distance from the cathode. This increase in distance improves the assumptions of quasineutrality and that the spatial diffusion of charged species is negligible. The region close to the cathode features complicated ion and electron buildup and as the relative distance from the cathode increases, its impact on the problem becomes negligible.

Table II summarizes the results obtained using the circuit model presented in this paper and associated experimental measurements made by Roupassov et al.[1] for both the "hot spot" and "tail" regions.

## IV. CONCLUSION

A new lumped element circuit model was presented that is valid for pulsed DC DBD plasmas. The model approximates the total energy dissipated into neutral species using a lumped element circuit while containing relevant plasma physics in the form of a variable electron temperature and number density. An approximate expression was formulated using the conductivity of the discharge to calculate the resistance value for the air gap. Asymmetric wall effects were also approximated in the model by including the effect of the anode sheath. Results of the model were verified against a pulsed DC experiment conducted by Roupassov et al.[1] and order of magnitude agreement was obtained for the energy imparted into the plasma in both the homogeneous "hot spot" region and "tail" region.

## ACKNOWLEDGMENTS

## APPENDIX: CROSS-SECTION DATA

The momentum cross sections used for the numerical approximations in the model are shown in Table III. These values were obtained by A. V. Phelps.[6]

TABLE III. Momentum cross sections.[6]

| Kinetic energy (eV) | N$_2$ ($10^{-16}$cm$^2$) | O$_2$ ($10^{-16}$cm$^2$) |
|---------------------|--------------------------|--------------------------|
| 1                   | 10                       | 7.2                      |
| 2.1                 | 27                       | 6.6                      |
| 3                   | 21.7                     | 5.7                      |
| 4                   | 12.6                     | 5.5                      |
| 5                   | 10.9                     | 5.6                      |
| 10                  | 10.4                     | 5                        |
| 15                  | 11                       | 8.8                      |
| 20                  | 10.2                     | 8.6                      |

[1] A. Y. Starikovskii, A. A. Nikipelov, M. M. Nudnova, and D. V. Roupassov, "SDBD plasma actuator with nanosecond pulse-periodic discharge," Plasma Sources Sci. Technol. **18**, 034015 (2009).

[2] D. Orlov, "Modelling and simulation of single dielectric barrier discharge plasma actuators," In: Aerospace and Mechanical Engineering. University of Notre Dame; 2006.

[3] D. J. Griffiths, *Introduction to Electrodynamics*, 3rd ed. (Prentice Hall, Upper Saddle River, NJ, 1999).

[4] M. Mitchner, *Partially Ionized Gases* (John Wiley & Sons, Inc., Indianapolis, IN, 1973).

[5] B. M. Smirnov, *Physics of Ionized Gases* (Wiley, New York, 2001).

[6] S. A. Lawton and A. V. Phelps, "Excitation of the b [sup 1] sigma [sup +][sub g] state of o[sub 2] by low energy electrons," J. Chem. Phys. **69**, 1055–1068 (1978).

[7] D. Orlov, T. Corke, and M. Patel, "Electric circuit model for aerodynamic plasma actuator," AIAA, paper no. 2006–1206, 2006.

[8] L. C. Pitchford, J. P. Boeuf, and W. L. Morgan, "User-friendly boltzmann code for electrons in weakly ionized gases," in IEEE International Conference on Plasma Science, 1996 IEEE Conference Record-Abstracts (1996), p. 154.

[9] Y. P. Raizer, *Gas Discharge Physics*, (Springer, 1991).

[10] G. W. Collins, "Fundamental numerical methods and data analysis," NASA Astrophysics Data System, 1990, http://ads.harvard.edu/books/1990fnmd.book/.

[11] I. V. Adamovich, M. Nishihara, I. Choi, M. Uddi, and W. R. Lempert, "Energy coupling to the plasma in repetitive nanosecond pulse discharges," Phys. Plasmas **16**, 113505 (2009).

[12] C. L. Enloe, T. E. McLaughlin, R. D. Van Dyken, K. D. Kachner, E. J. Jumper, T. C. Corke, M. Post, and O. Haddad, "Mechanisms and responses of a dielectric barrier plasma actuator: Geometric effects," AIAA J. **42**, 595–604 (2004).